

1 **Study on the removal and adsorption kinetics of malachite green in water by NaY molecular**  
2 **sieve prepared from coal gangue**

3

4 Qingping Wang <sup>1,2,3</sup>, Jing Min <sup>1</sup>, Wei Xu <sup>1</sup>

5 <sup>1</sup> School of Materials Science and Engineering, Anhui University of Science and Technology,  
6 Huainan 232001, China

7 <sup>2</sup>Anhui Industrial Generic Technology Research Center for New Materials from Coal-Based Solid  
8 Wastes, Anhui University of Science and Technology, Huainan 232001, China

9 <sup>3</sup>State Key Laboratory of Mining Response and Disaster Prevention and Control in Deep Coal Mines,  
10 Anhui University of Science and Technology, Huainan 232001, China

11 \*Corresponding author: Qingping Wang

12 E-mail: [wqp.507@163.com](mailto:wqp.507@163.com); Tel: [19555402142](tel:19555402142)

13 **ABSTRACT**

14 The synthesis of NaY molecular sieve from coal gangue and its adsorption properties for malachite  
15 green were studied. The process adopts high-temperature sintering hydrothermal method, which not  
16 only improves the utilization rate of coal gangue, but also analyzes the key parameters affecting the  
17 formation of molecular sieve with high adsorption efficiency of organic pollutants, and characterizes  
18 the materials by XRD, SEM, EDS, BET, etc. The adsorption process of malachite green solution was  
19 analyzed by adsorption kinetics and isotherm, and the adsorption mechanism was elucidated by XRD,  
20 FTIR, XPS and SEM. The results show that the maximum adsorption capacity of NaY molecular  
21 sieve for malachite green is 1910mg/g under the best conditions, which conforms to the quasi-second-  
22 order kinetic equation and Langmuir isothermal adsorption model.

23 **Keywords:** gangue, NaY molecular sieve, hydrothermal method, MG adsorption

24

## 25 **1. Introduction**

26 Water pollution has always been a major issue of global concern, especially printing and dyeing  
27 wastewater containing organic dyes (Dhaouefi et al. 2022). Malachite green (MG), as a typical  
28 alkaline and cationic dye, has a strong bactericidal ability, and even at lower concentrations it can act  
29 as a good inhibitor of bacteria (Guo et al. 2020), which is widely used in the aquaculture industry  
30 (Gavrilenko et al. 2019). However, due to the continuous accumulation of MGs in water bodies, they  
31 can damage water ecosystems, jeopardize the safety of water resources and affect the stability of  
32 aquatic ecosystems (Lin et al. 2022). To remove this toxic dye, various adsorption methods have been  
33 investigated, including photocatalytic oxygenation (Aswathy, JiJi, and Kumar 2022), chemical  
34 precipitation (Wang et al. 2022), adsorption (Gong et al. 2021). Among them, the adsorption method  
35 is considered as one of the most effective routes due to its ease of operation, absence of secondary  
36 pollution, and high removal rate (Shi et al. 2017) Adsorption. Kezhou Yuan et al. (Yan et al. 2023) A  
37 magnetic adsorbent made of CG was used to treat heavy metal ions in gold industry wastewater. It  
38 was found that the rate of adsorption of heavy metals Pb(II), Cd(II) and Cu(II) by this magnetic  
39 material was more than 70%. Hao Zhang et al (Zhang et al. 2022) synthesized ammonium  
40 Phosphotungstic /CG (NH<sub>4</sub>-PW/CG) through a simple precipitation method using gangue as the  
41 carrier. The adsorption efficiency of ciprofloxacin (CIP) exceeded 82% within 10 minutes. Xue Ma  
42 et al (Ma et al. 2023) prepared ZSM-5/CLCA molecular sieves from gangue using cellulose aerogel  
43 (CLCA) as the raw material and cellulose aerogel (CLCA) as the green templating agent using  
44 hydrothermal method. By studying the optimal conditions and reaction mechanism of product  
45 synthesis, it was proved that the material had good adsorption performance for malachite green, and  
46 the adsorption amount was 136.5 mg/g.

47 Coal gangue is a type of solid waste generated during coal mining and coal washing processes. It's a  
48 rock with a dark grey color. low carbon content and harder than coal, and it is an important solid  
49 waste for the development and utilization of China's coal resources, accounting for about 15-20% of  
50 the total amount of raw coal( (Zheng et al. 2024). In recent years, with the rapid growth of China's  
51 economy and the surging demand for coal power, China has been the world's largest coal producer  
52 and consumer (Haibin and Zhenling 2010) The amount of coal gangue stockpiles has exceeded 5  
53 billion tones. The accumulation of large amounts of coal gangue has resulted in the depletion of land  
54 resources, causing landslides, mudslides and other geological disasters, and bringing many adverse  
55 effects on local water, soil and air (Ge et al. 2020), It also poses a great threat to human health (Yun  
56 et al. 2016). The accumulation of the rock has caused the depletion of land resources and the  
57 occurrence of geological disasters such as landslides and mudslides, which have brought many  
58 adverse effects on the local water, soil and air. In recent years, researchers have been exploring and  
59 practice the use of coal gangue. Currently, people use coal gangue as mine backfill, road additives,  
60 and also made into agricultural fertilizer and flocculant (Gao et al. 2023). The gangue is also used in  
61 the fields of power generation, building materials production and land reclamation (Wu et al. 2024).  
62 However, this "low value-added" utilization has once again caused the waste of mineral resources (Li  
63 and Wang 2019). How to achieve high value-added use of coal gangue has become a hot research  
64 topic. Under China's current environmental protection strategy, this is one of the green upgrades  
65 urgently needed by the industry. Synthesis of zeolite molecular sieve from gangue as raw material  
66 will be one of the new uses of gangue.

67 Na-Y molecular sieves were synthesized for environmental remediation using an alkali-soluble  
68 hydrothermal method with coal gangue as the primary material. This approach not only significantly

69 reduced waste emissions but also enhanced the overall utilization of solid waste. The study explored  
70 the potential of producing Na-Y molecular sieves from coal gangue, which is rich in silicon and  
71 aluminum, and experimentally determined the optimal parameters for their synthesis. To understand  
72 the adsorption mechanisms of the molecular sieves on contaminants, various adsorption experiments  
73 were conducted. These included tests on different conditions, such as molecular sieve concentration  
74 and pH levels, as well as the application of adsorption kinetic models.

## 75 **2 Experimental**

### 76 *2.1 Experimental reagents*

77 The gangue sourced from Huainan City, Anhui Province, China, served as the aluminum and silicon  
78 sources for the experiments. Sodium hydroxide (NaOH, AR,  $\geq 99.70\%$ ) was procured from  
79 Sinopharm Chemical Reagent Co. Ltd, The pure water used in the experiment was self-made  
80 deionized water. All reagents employed in this study were of analytical grade and did not undergo  
81 any pretreatment experimental methodology.

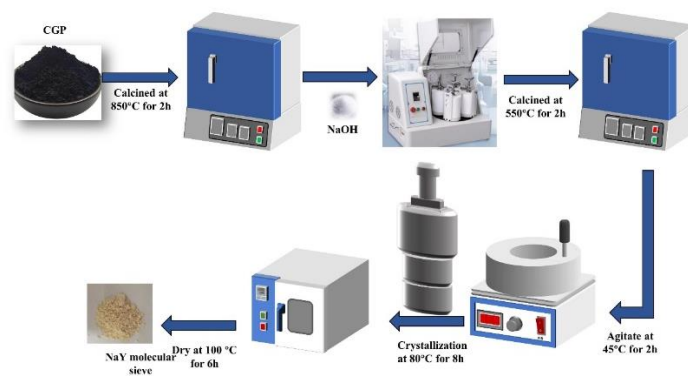
### 82 *2.2 Preparation of molecular sieves*

83 NaY molecular sieves were synthesized via a conventional hydrothermal method, as illustrated in  
84 Figure 1. Initially, gangue was calcined at 850 °C in an open ceramic crucible. After reaching the  
85 desired roasting temperature, the crucible was left in the furnace for 2 h and then cooled to room  
86 temperature. Subsequently, the calcined gangue was uniformly mixed with NaOH in a ball milling  
87 jar at a mass ratio of 1:1.2. The mixture was then subjected to further calcination at 500 °C for 2 h to  
88 obtain the alkali-soluble product, as depicted in steps (1) and (2) of the alkali-soluble process (Kong  
89 and Jiang 2021) :



91 
$$\text{Al}_2\text{O}_3 \cdot 2\text{SiO}_2 + 2\text{NaOH} = 2\text{NaAlSiO}_4 + \text{H}_2\text{O} \quad (2)$$

92 Following this, 6.59 g of alkali-soluble product, 0.84 g of hydroxide, and 60 ml of deionized water  
93 were sequentially added to a beaker and age at 45 degrees for 10 h. After thorough aging, the raw  
94 material was transferred into a stainless steel container lined with polytetrafluoroethylene and placed  
95 in an oven at 80 °C for 10 h. Finally, the sample was cooled, filtered, washed to neutrality, and dried  
96 in a vacuum drying oven at 100 °C for 6 h.



97  
98 **Figure 1.** Process flow diagram of Nay molecular sieve synthesis from gangue.

### 99 2.3 Adsorption Experiment of MG

100 20 mg of MG powder was added to a 250 ml beaker, followed by filling with 100 ml of deionized  
101 water and stirring at 500 rpm for 0.5 h in a thermostatic water tank to ensure complete dissolution of  
102 the MG. After dissolution, the solution was transferred to a 1 L volumetric flask to determine the  
103 volume, resulting in an MG stock solution of 200 mg/L. The absorbance of the solution was measured  
104 at 617 nm by UV-VIS spectrophotometer. The MG standard curve is shown in Figure 2.

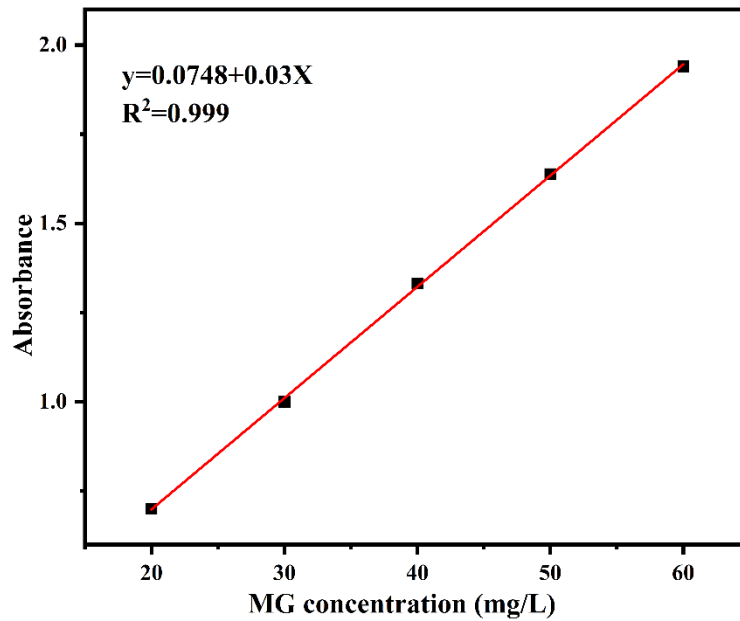


Figure 2. MG standard curve.

105  
106

107 The prepared molecular sieve was used for the adsorption test of MG. After adsorption, the  
108 adsorbent is separated from the MG solution using a high-speed centrifuge. The absorbance of the  
109 solution before and after adsorption was recorded by UV-VIS spectrophotometer. The formulas for  
110 calculating the adsorption capacity and removal rate of dyes are shown in (3):

$$111 \quad Q_e = \frac{(C_0 - C_e) * V}{W} \quad (3)$$

112 In the formula,  $Q_e$  is the adsorption capacity (mg/L);  $C_0$ ,  $C_e$  are the concentration of MG in solution  
113 before and after adsorption (mol/L), respectively;  $V$  is the volume of MG in the experiment;  $W$  is the  
114 amount of molecular sieve (g);  $n$  is the removal rate of MG in solution.

#### 115 2.4 Characterization

116 The raw material composition and content of coal gangue were analyzed by ARL-9800 X-ray  
117 fluorescence spectroscopy (XRF). The crystal patterns and characteristics of the samples were  
118 analyzed by Shimadzu XRD-6000 X-ray diffractometer. The micromorphology of the samples was  
119 analyzed using an electron microscope (SEM, ZSISS Sigma 300), and the surface elements were  
120 analyzed by energy dispersive spectrometry (EDS). Bruker's IFS88 Fourier transform infrared

121 spectrometer FT-IR was used to analyze the functional groups of the samples, and the wave number  
122 was selected in the range of 4000-400cm<sup>-1</sup>. X-ray electron spectroscopy (XPS) of ESCALB Xi<sup>+</sup> was  
123 used to study the adsorption mechanism. Finally, at -196°C, the N<sub>2</sub> adsorption-desorption isotherm  
124 of the sample was determined using the Micromeritics ASAP 2020 analyzer (Micromeritics,  
125 Norcross, GA, USA) to assess its surface area and pore size.

### 126 3 Results and Discussion

#### 127 3.1 Gangue analysis

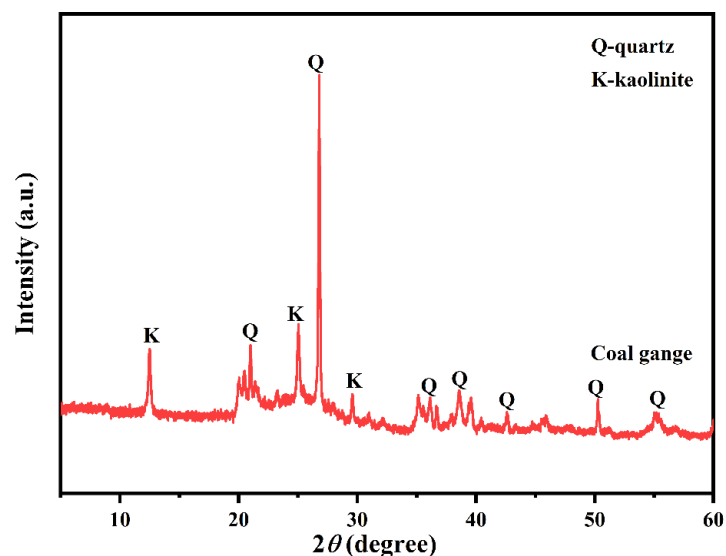
128 The main chemical composition (wt.%) of the gangue was determined by X-ray fluorescence  
129 spectroscopy (XRF), and the results are presented in Table 1. Based on the wt.% values listed in Table  
130 1, the molar ratio of SiO<sub>2</sub>/Al<sub>2</sub>O<sub>3</sub> in the gangue was calculated to be approximately 3.1. This ratio  
131 indicates that the gangue can serve as a source of pure silicon and aluminum for synthesizing Nay  
132 molecular sieves.

133 **Table 1.** Main chemical composition in gangue (wt.%)

SiO <sub>2</sub>	Al <sub>2</sub> O <sub>3</sub>	Fe <sub>2</sub> O <sub>3</sub>	CaO	MgO	NaO <sub>2</sub>	TiO <sub>2</sub>	other than
55.62	30.43	6.37	2.47	1.05	0.9	0.92	2.24

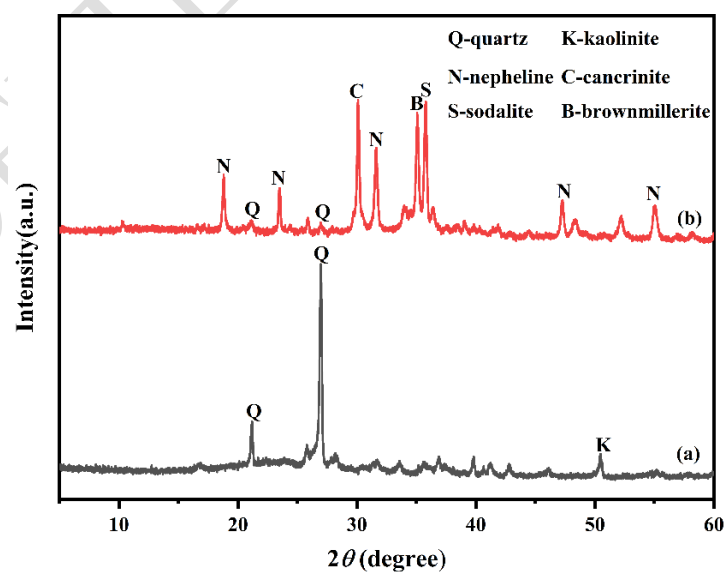
134 It can be seen from the XRD pattern (as shown in Figure 3) that the main mineral components of coal  
135 gangue are quartz and kaolinite, the structure is stable and the activity is low. Therefore, coal gangue  
136 raw material can not meet the raw material requirements for preparing Nay molecular sieve. Before  
137 the hydrothermal reaction, the coal gangue needs to be further activated.





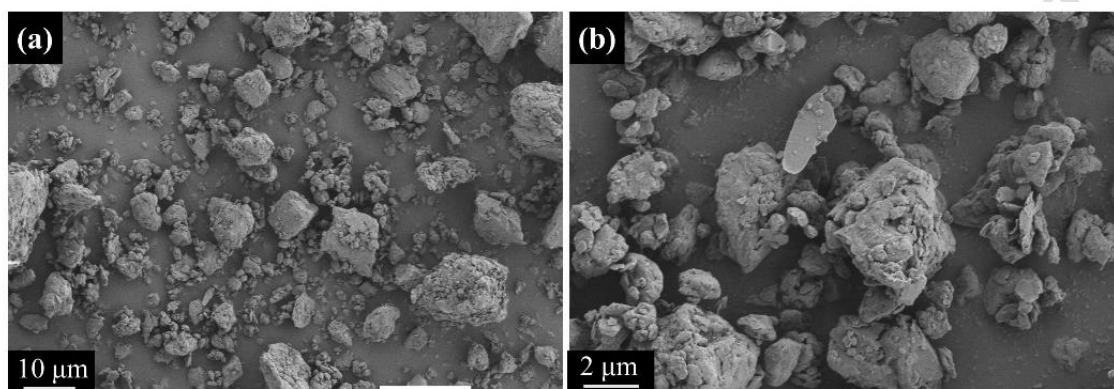
138  
139 **Figure 3.** XRD spectra of gangue raw samples.

140 The X-ray diffraction (XRD) pattern of coal gangue following high-temperature calcination and alkali  
141 melting is illustrated in Figure 4. Analysis of this Figure reveals that the characteristic peak of  
142 kaolinite disappears during the alkali melting process. Additionally, the intensity of the quartz peak  
143 is notably reduced. In contrast, new crystalline phases such as muscovite, calcite, sodalite, and  
144 calcium ferrite emerge. These phases exhibit higher reactivity, which enhances the potential for  
145 synthesizing molecular sieves in subsequent hydrothermal reactions.



146  
147 **Figure 4.** XRD pattern of coal gangue after calcination(a); XRD pattern of alkali dissolved coal  
148 gangue(b).

149 Scanning electron microscopy was used to analyze the microscopic morphology of coal gangue. As  
150 shown in Figure 5, it can be seen that coal gangue raw materials are irregular lumps or aggregates  
151 with uneven particle size distribution and significant amorphous particulate matter appearing on the  
152 surface.



153

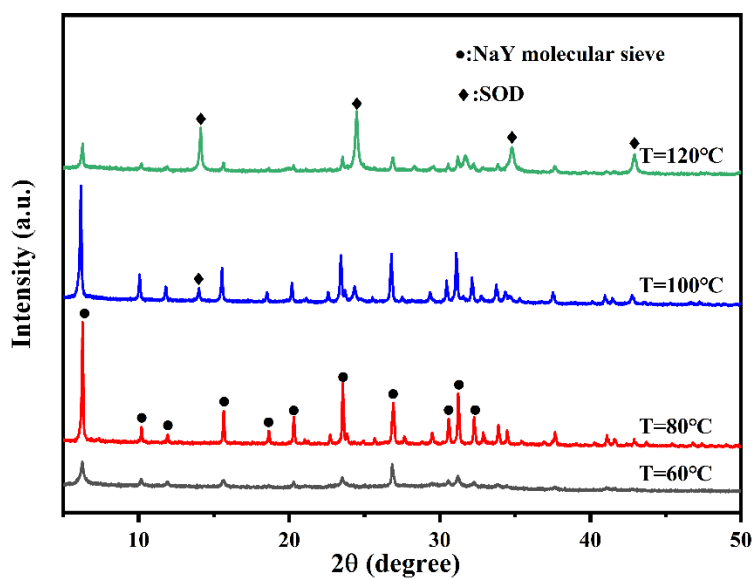
154

**Figure 5.** SEM image of gangue original sample.

155 *3.2 Effect of preparation conditions on the synthesis of Nay molecular sieves*

156 *3.2.1 Effect of crystallization temperature*

157 In this phase, XRD analysis was conducted on Nay molecular sieves synthesized at various  
158 crystallization temperatures over a period of 8 hours, as shown in Figure 6. At lower temperatures,  
159 the energy available for the reaction is limited, resulting in minimal formation of crystalline phases  
160 in the synthetic products. In a closed reactor, fluctuations in crystallization temperature can cause  
161 pressure changes, which in turn affect the nucleation and growth processes of the sample, leading to  
162 variations in the crystallization product's structure. Figure 6 indicates that once the reaction  
163 temperature exceeds 80 °C, both the characteristic diffraction peak and the overall crystallinity of the  
164 synthesized product start to decline as the temperature rises. Additionally, the emergence of other  
165 crystal types on the surface of the product and the formation of nerite are observed at these higher  
166 temperatures. Therefore, the optimal crystallization temperature is identified as 80 °C.



168

169 **Figure 6.** XRD patterns of NaY molecular sieves synthesized at different crystallization

170

temperatures.

171 *3.2.2 Effect of crystallization time crystallization*

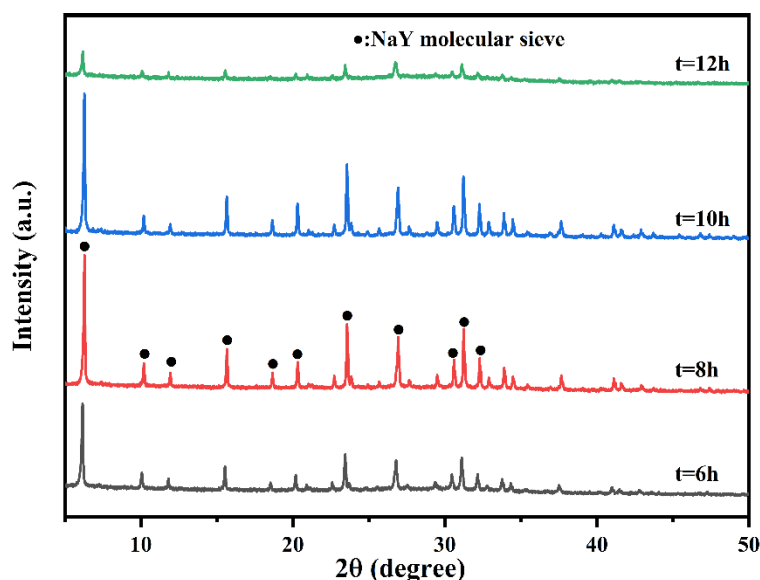
172 The XRD patterns of NaY zeolite synthesized at 80 °C with varying crystallization times are depicted

173 in Figure 7. It is evident from Figure 7 that the intensity of the diffraction peaks of the synthesized

174 sample is highest when the crystallization time is 8 h. Additionally, the characteristic diffraction peak

175 of the create sample corresponds to the diffraction peak of the standard PDF card 43-0168, indicating

176 that the synthesized sample at this crystallization temperature is a typical NaY molecular sieve.

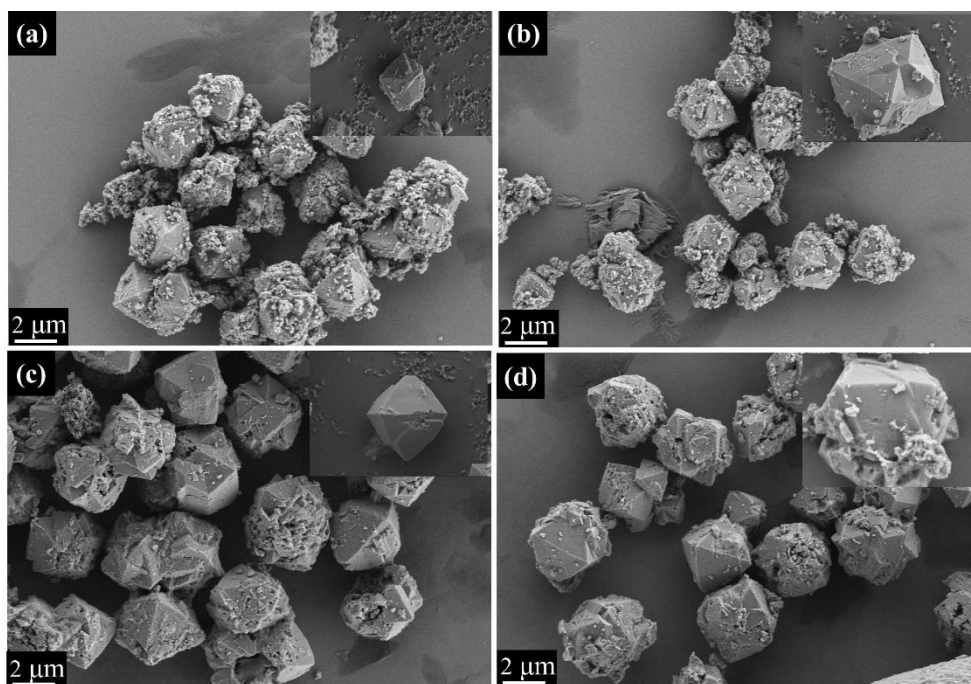


177

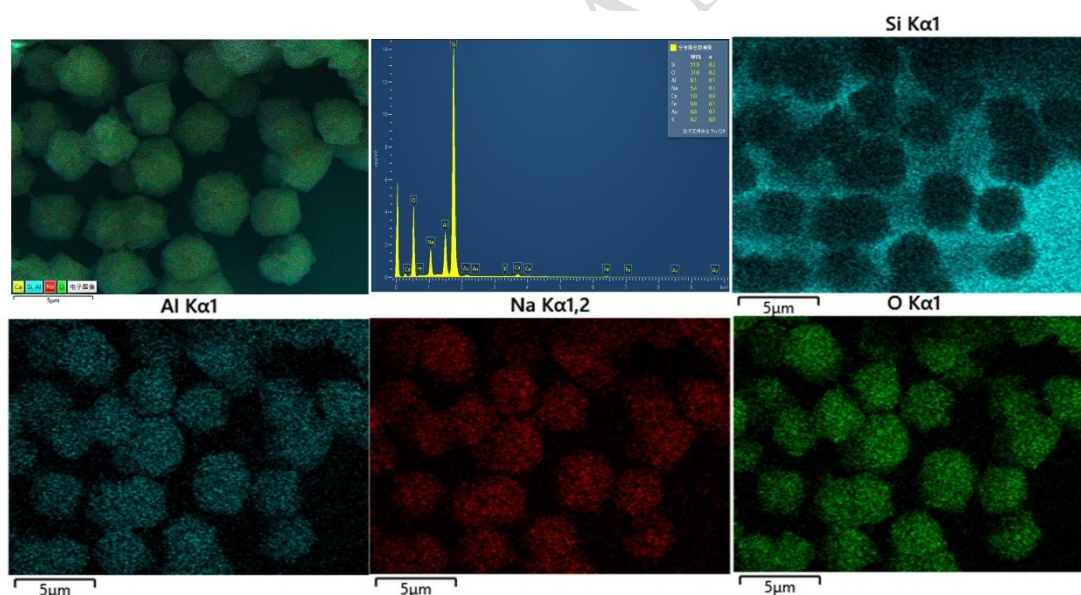
178 **Figure 7.** XRD patterns of NaY molecular sieves synthesized at different crystallization times.

179 *3.3 Scanning analysis*

180 In Figures 8 (a ~ d), SEM images show the development of Na-Y zeolite at various crystallization  
 181 times. The images reveal that octahedral nuclei of the Na-Y molecular sieve begin to form at different  
 182 time intervals. At the 6-hour mark, some unreacted raw materials are still visible. However, after  
 183 extending the crystallization time to 8 hours, the sample exhibits a well-defined octahedral structure  
 184 with a smooth and intact surface, measuring approximately 2  $\mu\text{m}$  in size. Figure 9 presents the surface  
 185 composition of the prepared Na-Y molecular sieve, analyzed through SEM-EDS. The distribution of  
 186 elements—silicon, aluminum, sodium, and oxygen—appears uniform across the surface of the  
 187 molecular sieve. The EDS spectrum further confirms the presence of these main elements, providing  
 188 consistency in the analysis.



189  
 190 **Figure 8.** SEM images of synthesized NaY molecular sieves with different crystallization  
 191 times:(a) 6 h; (b) 8 h; (c) 10 h; (d) 12 h.

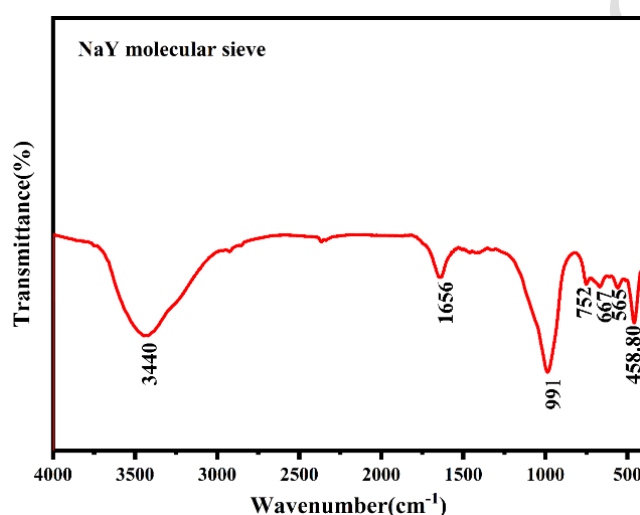


192  
 193 **Figure 9.** EDS spectra of NaY molecular sieve.

194 *3.4 FT-IR analysis*

195 The infrared spectrum of NaY molecular sieve is shown in Figure 10. In the synthesized products,  
 196 characteristic absorption peaks near  $1656\text{ cm}^{-1}$  and  $991\text{ cm}^{-1}$  represent the O-H bending vibration of  
 197 water molecules and the asymmetric stretching vibration of Si-O bonds, respectively. The absorption

198 peak near  $752\text{ cm}^{-1}$  is attributed to the stretching mode of tetrahedral atoms, while the peak near  $667$   
199  $\text{cm}^{-1}$  corresponds to the Al-O symmetric stretching vibration. Furthermore, characteristic absorption  
200 peaks arising from double hexagonal ring vibrations are noted around  $565\text{ cm}^{-1}$  when Al is in an  
201 octahedral coordination state (Rao et al. 2023), and the bending vibration of the tetrahedral Si-O-Al  
202 chain leads to characteristic peaks near  $458\text{ cm}^{-1}$ . These findings confirm the successful conversion  
203 of gangue into Nay molecular sieves, as evidenced by characterization techniques including X-ray  
204 diffraction, scanning electron microscopy, and infrared spectroscopy.



205  
206 **Figure 10.** FT-IR spectra of Nay molecular sieves.

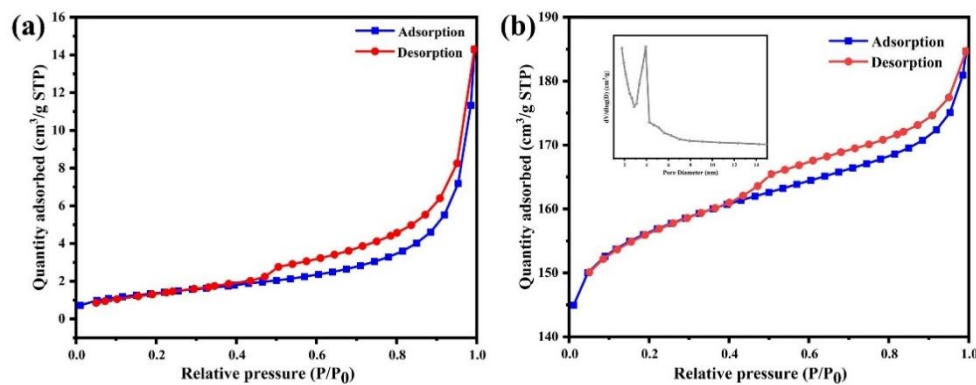
### 207 3.5 Specific surface area analysis

208 BET specific surface area analysis is a widely used method for characterizing the pore structure of  
209 solid materials, based on the adsorption of gases on solid surfaces. This analysis uses adsorption  
210 isotherm data to examine the material's pore structure. According to Table 2, the specific surface area  
211 of gangue is only  $5.0\text{ m}^2/\text{g}$ , suggesting that the raw gangue material has a very weak adsorption  
212 capacity. Conversely, the BET specific surface area of the Nay molecular sieve, synthesized through  
213 a hydrothermal reaction, reaches  $621.92\text{ m}^2/\text{g}$  with an average pore size of  $4.69\text{ nm}$ . The BJH curve  
214 depicted in Figure 11b shows that the Nay zeolite possesses a microporous and mesoporous structure,

215 with the pore size predominantly concentrated around mesopores of 4.69 nm. According to the  
 216 IUPAC classification standards, the isotherm curve of the NaY molecular sieve can be categorized as  
 217 a Type IV curve, primarily characteristic of mesoporous materials. This type of isotherm reflects  
 218 multilayer adsorption on the surfaces of non-porous homogeneous solids and is indicative of a typical  
 219 physical adsorption process.

220 **Table 2.** Surface structure parameters of NaY molecular sieve

	Specific surface area (BET) m <sup>2</sup> /g	Pore volume m <sup>3</sup> /g	Particle stacking pore size nm
waste rock (in coal mining)	5.00	-	-
NaY molecular sieve	621.92	0.21	4.69



221  
 222 **Figure 11.** N<sub>2</sub> adsorption-desorption isotherm curve of coal gangue(a); N<sub>2</sub> adsorption-desorption  
 223 isotherm curve and pore size distribution of NaY molecular sieve(b).

### 224 3.6 Adsorption performance analysis

#### 225 3.6.1 Adsorption kinetics

226 The adsorption process of MG by NaY molecular sieve can be described by quasi-first-order (Eq.(4)),  
227 quasi-second-order (Eq.(5)) and intra-particle diffusion model (Eq.(6)).

$$228 \quad \ln(q_e - q_t) = \ln q_e - k_1 t \quad (4)$$

$$229 \quad \frac{t}{q_t} = \frac{1}{K_2 q_e^2} + \frac{1}{q_e} t \quad (5)$$

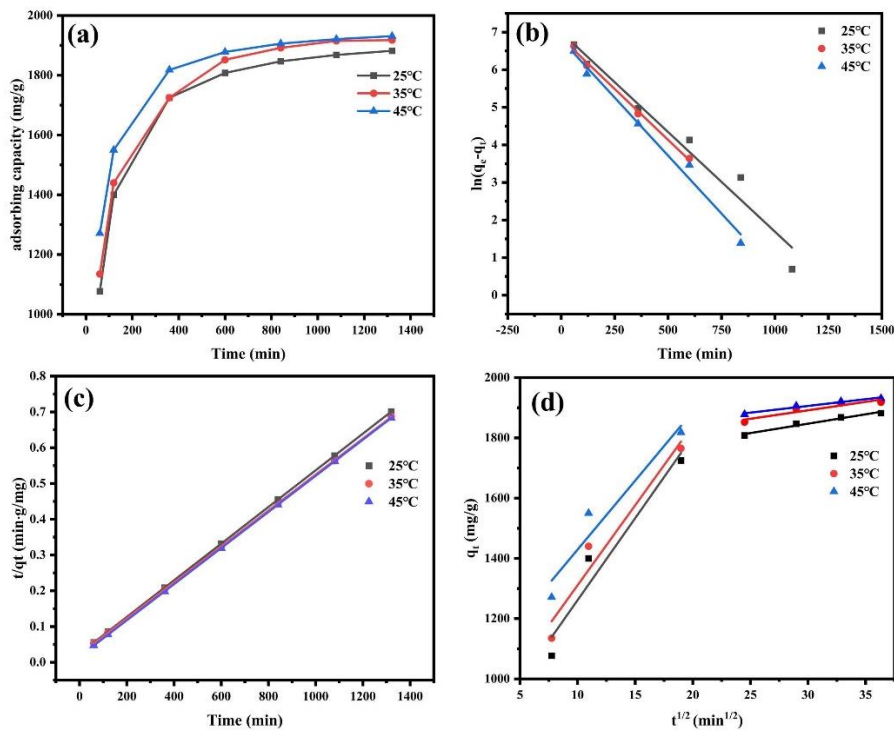
$$230 \quad q_t = k_t t^{\frac{1}{2}} + C \quad (6)$$

231 In the formula,  $q_e$  and  $q_t$  are respectively the adsorption capacity of MG at 1380 (min) and the  
232 adsorption capacity of  $t$  (min) time (mg/g);  $k_1$  ( $\text{min}^{-1}$ ),  $k_2$ [g/(min·mg)] and  $k_{id}$ [mg/(g/min<sup>1/2</sup>)] are the  
233 rate constants of the quasi-first-order kinetic equation, the quasi-second-order kinetic equation and  
234 the rate of intra particle diffusion, respectively.  $C$  is the adsorption constant;  $t$  is the adsorption time  
235 (min).

236 In order to investigate the adsorption rate of NaY molecular sieve for MG, 10 MG NaY molecular  
237 sieve was added to 100 mL MG solution with a concentration of 200 MG /L. Adsorption rates were  
238 measured at temperatures of 25°C, 35°C and 45°C. As shown in Figure 12a, the adsorption rate  
239 gradually decreases with the increase of adsorption time, while the adsorption rate and capacity  
240 increase with the increase of temperature. The kinetic fitting results are displayed in Figure 12b、c,  
241 and summarized in Table 3. As indicated in Table 3, the correlation coefficients of the pseudo-second-  
242 order kinetic model are significantly higher than those of the pseudo-first-order model across all  
243 temperatures. Moreover, the saturation adsorption capacities predicted by the pseudo-second-order  
244 model align more closely with the experimental values, suggesting that the adsorption of MG onto  
245 the NaY molecular sieve at various temperatures follows a pseudo-second-order kinetic model. This  
246 implies that the primary adsorption mechanism is chemisorption (Meena, Kukreti, and Jassal 2024).  
247 As shown in Figure 12d, all fitted curves appear as straight lines that do not pass through the origin,



248 indicating that the intercept C is not equal to zero. Additionally, Table 3 shows that while the fitted  
 249 curves exhibit a strong linear relationship, they do not intersect the origin. These observations suggest  
 250 that, beyond internal diffusion, multiple mechanisms influence the adsorption of MG onto the  
 251 molecular sieve (Li et al. 2023).



252  
 253 **Figure 12.** the impact of time on MG (a) ;Quasi-first-order kinetic curve(b) ;Quasi-second-order  
 254 kinetic curve (c); Intraparticle diffusion model curve(d).

255 **Table 3.** Fitting parameters of adsorption kinetics.

Kinetic models	Parameters	Temperature 25 °C, 35 °C, 45 °C		
	$q_{e,ecp}$	1877	1890	1910
	$q_{e1}$ (mg/g)	1099	940	900
quasi-first-orde	$k_1$ (min <sup>-1</sup> )	0.0053	0.0054	0.0062
	$R^2$	0.9558	0.9929	0.9819
	$q_{e2}$ (mg/g)	1960	1988	1990

Pseudo-	$k_2$ (g/(mg·min))	0.00011	0.000113	0.00015
second-order	$R^2$	0.999	0.999	0.999
	$K_{t1}$ (mg/(g/min) <sup>1/2</sup> )	54.43	53.13	45.79
	$C_1$	777	779	971
Intra-particle	$R_1^2$	0.8857	0.9006	0.8730
Diffusion	$K_{t2}$ (mg/(g/min) <sup>1/2</sup> )	6.22	5.62	4.46
	$C_2$	1660	1722	1772
	$R_2^2$	0.9556	0.8298	0.9549

### 256 3.6.2 Adsorption isotherms

257 The adsorption data were simulated with the Langmuir model (Eq. (7)) (Mahreni et al. 2022) and the  
 258 Freundlich model (Eq. (8)) (Uyiosa Osagie et al. 2021).

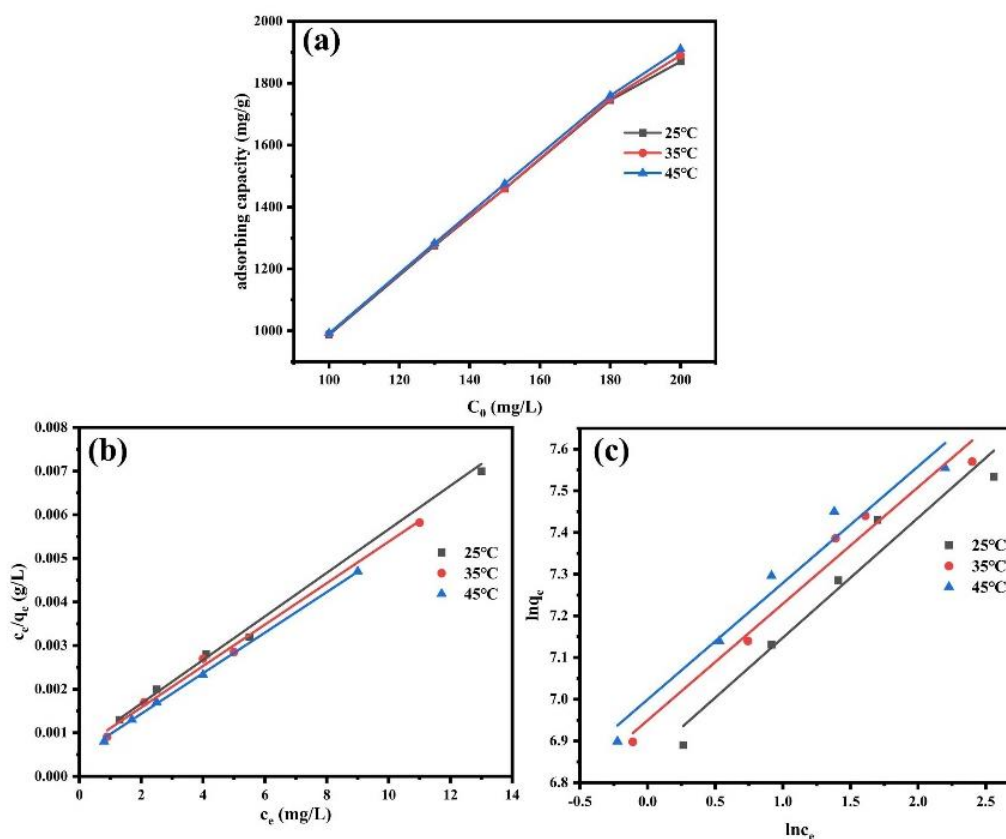
$$259 \frac{C_e}{q_e} = \frac{C_e}{q_{max}} + \frac{1}{K_L q_{max}} \quad (7)$$

$$260 \ln q_e = \ln K_f + \frac{1}{n} \ln C_e \quad (8)$$

261 Where  $q_{max}$  (mg/g) means maximum saturated adsorption amount,  $K_L$  (L/mg) refers to the Langmuir  
 262 constant,  $K_F$  (mg/g) represents the adsorption coefficient and  $1/n$  means Freundlich constants.

263 To evaluate the isothermal adsorption process, 10 mg of NaY molecular sieve was introduced into  
 264 100 mL of MG solution at varying concentrations. The equilibrium adsorption behavior was  
 265 examined at temperatures of 25°C, 35°C, and 45°C. Figure 13a illustrates the adsorption isotherms  
 266 of the NaY molecular sieve for MG across different temperatures and concentrations, offering  
 267 insights into the adsorption characteristics under these conditions. Figure 13b, c present the analysis  
 268 of adsorption behavior using the Langmuir and Freundlich isotherm models, with the

269 derived parameters detailed in Table 4. For NaY molecular sieve, the adsorption capacity increased  
270 as the initial concentration of MG rose, and showed a slight enhancement with elevated  
271 temperatures. The increase in adsorption at higher temperatures suggests that the adsorption of MG  
272 onto NaY zeolite is an endothermic process. The fitting correlation coefficients  $R^2$  (0.9967、 0.9923  
273 、 0.9990) of the Langmuir isothermal model at different temperatures were higher than those of the  
274 Freundlich isothermal adsorption model,. This suggests that the adsorption of MG onto the NaY  
275 molecular sieve follows a monolayer adsorption mechanism. While the Freundlich isotherm model  
276 can describe the adsorption process in certain scenarios, the Langmuir model exhibits a stronger  
277 correlation with the NaY molecular sieve data in this experiment, providing a more accurate  
278 interpretation of the adsorption behavior. In addition, Table 5 shows the comparison of adsorption  
279 of MG by different adsorbents synthesized from solid wastes. It can be seen that the NaYmolecular  
280 sieve synthesized from solid waste has a high specific surface area and good MG adsorption  
281 performance. However, there is no research on synthesizing NaYmolecular sieve for MG adsorption  
282 using coal gangue. Additionally, Table 5 presents a comparison of MG adsorption performance by  
283 various adsorbents derived from solid wastes. It is evident that the NaY molecular sieve synthesized  
284 from solid waste exhibits a high specific surface area and excellent MG adsorption capacity.  
285 However, there is a lack of studies on the use of coal gangue to synthesize NaY molecular sieves



287

288 **Figure 13.** Adsorption isotherm of NaY molecular sieve to MG (a) ;Langmuir model (b) and

289 Freundlich model(c).

290 **Table 4.** The parameters of adsorption isotherms.

Kinetic models	Parameters	Temperature 25 °C, 35 °C, 45 °C		
Langmuir model	$q_m$ (mg/g)	2078	2106	2123
	$K_L$ (L/mg)	0.6687	0.7683	0.9942
	$R_2$	0.9967	0.9923	0.9990
Freundlich model	$K_F$ (mg/g)	940	1050	1100
	$1/n$	0.2801	0.2721	0.2698
	$R^2$	0.9653	0.9592	0.9519

291 **Table 5.**Summary of literature on the specific surface area and MG adsorption of ad-

Raw	Adsorbent	Specific surface area ( $\text{m}^2\text{g}^{-1}$ )	Adsorption capacity (mg $\text{g}^{-1}$ )	Reference
Coal gasification slag	ZSM-5	299	80	(Yuan et al. 2022)
Fly ash	Flyash molecular sieve	404	32	(Zgureva et al. 2020)
Coal gangue	ZSM-5	398	136.5	(Ma et al. 2023)
Metakaolin	Zeolite A	/	55	(Pereira et al. 2018)

293 *3.6.3 Adsorption Thermodynamic Model*

294 The thermodynamics of adsorption is typically analyzed using key thermodynamic parameters, such  
 295 as enthalpy change ( $\Delta H$ ), entropy change ( $\Delta S$ ), and Gibbs free energy ( $\Delta G$ ). These functions  
 296 provide valuable insights into the nature and feasibility of the adsorption process. The calculation  
 297 formula is shown in equation (9), (10), (11) and (12) :

$$298 \quad K_c = C_{\alpha,e}/C_e \quad (9)$$

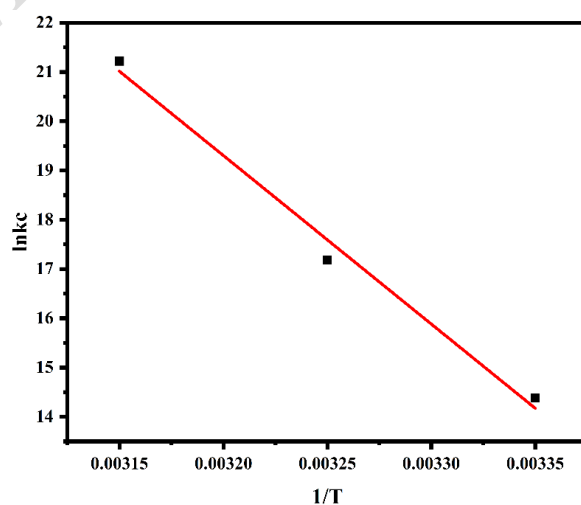
$$299 \quad \Delta G = RT \ln K_c \quad (10)$$

$$300 \quad \Delta G = \Delta H - T\Delta S \quad (11)$$

301 
$$\ln K_c = -\frac{\Delta H}{RT} + \frac{\Delta S}{R} \quad (12)$$

302 Where  $K_c$  represents the adsorption coefficient,  $C_e$  is the equilibrium concentration of MG molecules  
303 in the solution (mg/g), and  $C_{a,e}$  denotes the concentration of MG molecules on the adsorbent at  
304 equilibrium (mg/g).  $T$  is the absolute temperature (K), and  $R$  is the ideal gas constant, valued at 8.314  
305 J/(mol·K).  $\Delta H$  (enthalpy change,  $\text{kJ}\cdot\text{mol}^{-1}$ ),  $\Delta S$  (entropy change,  $\text{kJ}\cdot\text{mol}^{-1}$ ), and  $\Delta G$  (Gibbs free  
306 energy,  $\text{kJ}\cdot\text{mol}^{-1}$ ).

307 By plotting  $\ln K_d$  and  $1/T$  and performing linear fitting on the experimental data, Figure 14 was  
308 generated. Table 5 presents the calculated values of  $\Delta G$ ,  $\Delta S$  and  $\Delta H$ , and further interprets the  
309 direction, extent, and feasibility of MG adsorption based on their signs. As shown in Table 5, the  
310 positive value of  $\Delta H > 0$  suggests that the adsorption process is endothermic. The negative values of  
311  $\Delta G$  across different temperatures indicate that the adsorption of MG by the molecular sieve is  
312 spontaneous. Furthermore, the decrease in  $\Delta G$  with rising temperature implies that higher  
313 temperatures enhance the spontaneity of the process, thus favoring adsorption. The positive value of  
314  $\Delta S > 0$  suggests an increase in disorder within the reaction system, which further facilitates the  
315 adsorption of MG onto the NaY molecular sieve.



316

317 **Figure 14.** Thermodynamic fitting diagram of adsorption of MG by NAY-type molecular sieve.

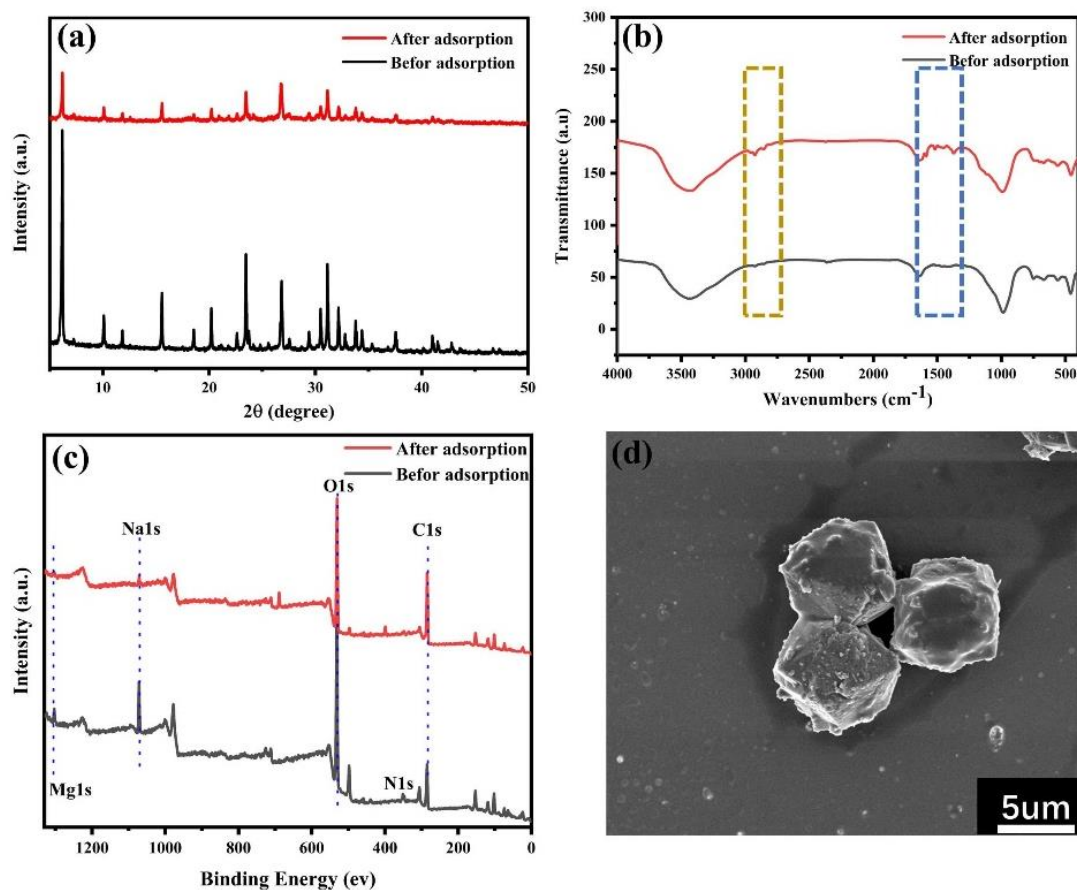
**Table 6.** Nay-type molecular sieve adsorption of MG thermodynamic parameters.

Temperature (°C)	Thermodynamic fitting parameters		
	$\Delta H$ (kJ/mol)	$\Delta S$ (J/(mol·K))	$\Delta G$ (kJ/mol)
25	-	-	-34.5
35	284.3	1070	-45
45	-	-	-55

319 *3.7 Adsorption mechanism analysis*

320 The adsorption mechanism of NaY molecular sieve on MG was studied by XRD, FT-IR, XPS and  
321 SEM. As can be seen from Figure 15a, the intensity of XRD diffraction peaks was significantly  
322 weakened after MG adsorption by the molecular sieve, while the typical X-ray diffraction peaks  
323 corresponding to NaY molecular sieve remained intact, indicating that the crystal structure of the  
324 molecular sieve was not destroyed after MG adsorption. FT-IR spectra of NaY molecular sieve before  
325 and after adsorption were given (FIG. 15b). It can be seen from Figure 15b that the characteristic  
326 peaks of MG dye molecules appear in the FT-IR spectra of 1600-1300<sup>-1</sup> and 2800-3000<sup>-1</sup> after  
327 adsorption, which proves that MG is adsorbed on the surface of the material. XPS analysis was  
328 performed on the molecular sieve before and after adsorption, and the results were shown in Figure  
329 15c. It can be seen that after MG adsorption, the characteristic peaks of Mg 1s and Na 1s at 1303.10eV  
330 almost disappear, indicating that the adsorption of MG is caused by ion exchange, mainly the  
331 exchange of dye cation and Na<sup>+</sup>. The morphologies of adsorbed samples were observed by scanning  
332 electron microscopy (SEM). The SEM image of the Nay-type molecular sieve after adsorption of MG  
333 shown in FIG. 15d shows that the original particle structure of the molecular sieve is basically intact,  
334 which is consistent with the peak shape retention observed in the XRD pattern of FIG. 15a. However,

335 the surface becomes noticeably rough, with many fine sheets of material attached to the previously  
336 smooth octahedral particles. These deposits may be MG dyes, further confirming that Nay-type  
337 molecular sieve successfully adsorbed dye molecules.



338  
339 **Figure 15.** XRD (a), FT-IR (b), and XPS (c) analyses of the NaY molecular sieve before and after  
340 adsorption; SEM image of molecular sieve after adsorption (d).

#### 341 4 Conclusion

342 The successful synthesis of NaY molecular sieve from coal gangue provides an effective way to  
343 increase the added value of solid waste and deal with environmental problems. Through the optimized  
344 hydrothermal process and alkali activation, the NaY molecular sieve obtained has a specific surface  
345 area of  $621.92 \text{ m}^2/\text{g}$  and an average pore size of  $4.69 \text{ nm}$ , which makes it excellent in the removal of  
346 malachite green, and the maximum adsorption capacity reaches  $1910 \text{ mg/g}$ . The adsorption process



347 follows the pseudo-second-order kinetic model and is in good agreement with the Langmuir  
348 isothermal model, which indicates that the main adsorption mechanism is chemisorption. The  
349 thermodynamic results show that the adsorption of MG is a spontaneous endothermic process. XRD  
350 、 FT-IR and XPS analysis proved that chemisorption (ion exchange) was the main mechanism of  
351 NaY molecular sieve adsorption of malachite green. These studies highlight the potential for  
352 synthesizing high-performance adsorbents from coal gangue to not only help reduce waste, but also  
353 aid in the remediation of contaminated water sources. Future work could explore scaling up the  
354 process and testing the material's effectiveness in real-world applications, which could lead to broader  
355 environmental benefits.

#### 356 **Author Contributions**

357 All authors have contributed to the study conception and design. “Conceptualization, Jing Min and  
358 Qingping Wang; validation, Wei Xu; investigation, Jing Min; data curation, Jing Min; writing—  
359 original draft, Jing Min; supervision, Qingping Wang; project administration, Qingping Wang.  
360 All authors have read and agreed to the published version of the manuscript.”

#### 361 **Acknowledgments**

362 This research was funded by National Natural Science Foundation of China (NSFC) [52227901];  
363 the University Synergy Innovation Program of Anhui Province [GXXT-2022-083], [GXXT-2023-  
364 019]; Anhui Provincial Natural Science Foundation [2208085ME103].

#### 365 **References**

- 366 Aswathy, N. R., Varghese Jiji, and R. Vinod Kumar. 2022. 'Photocatalytic degradation of malachite green using  
367 vanadium pentoxide-doped NiO thin film by sol-gel spin coating', *The European Physical Journal Plus*.  
368 <http://dx.doi.org/10.1007/s10653-021-01187-4>
- 369 Dhaouefi, Zaineb, Aida Lahmar, Rihab Khlifi, Imene Ben Toumia, Dorra Elgueder, and Leila Chekir-Ghedira  
370 . 2022. 'Evaluation of eventual toxicities of treated textile wastewater using anoxic-aerobic algal-b

371 bacterial photobioreactor', *Environmental Geochemistry and Health*. <http://dx.doi.org/10.1016/j.match>  
372 [emphys.2019.122240](http://dx.doi.org/10.1016/j.matchemphys.2019.122240)

373 Gao, J., Q. Lin, T. Yang, Y. C. Bao, and J. Liu. 2023. 'Preparation and characterization of ZSM-5 molecula  
374 r sieve using coal gangue as a raw material via solvent-free method: Adsorption performance te  
375 sts for heavy metal ions and methylene blue', *Chemosphere*, 341: 139741. <https://dx.doi.org/10.10>  
376 [16/j.chemosphere.2023.139741](https://dx.doi.org/10.1016/j.chemosphere.2023.139741)

377 Gavrilenko, N. A., T. N. Volgina, E. V. Pugachev, and M. A. Gavrilenko. 2019. 'Visual determination of malachite  
378 green in sea fish samples', *Food Chem*, 274: 242-45. <https://dx.doi.org/10.1016/j.foodchem.2018.08.139>

379 Ge, Q., M. Moeen, Q. Tian, J. Xu, and K. Feng. 2020. 'Highly effective removal of Pb(2+) in aqueous solution by  
380 Na-X zeolite derived from coal gangue', *Environ Sci Pollut Res Int*, 27: 7398-408.  
381 <https://dx.doi.org/10.1007/s11356-019-07412-z>.

382 Gong, Liang, Jie Wang, Chenhao Jiang, Teng Xiao, Kang Shen, Ming Lei, and Yiping Tang. 2021. 'Study on Magnetic  
383 Porous Carbon Microspheres as a Novel Adsorbent for Malachite Green', *ChemistrySelect*.  
384 <https://dx.doi.org/10.1002/slct.202100129>

385 Guo, Feiqiang, Xiaochen Jiang, Xiaolei Li, Xiaopeng Jia, Shuang Liang, and Lin Qian. 2020. 'Synthesis of  
386 MgO/Fe<sub>3</sub>O<sub>4</sub> nanoparticles embedded activated carbon from biomass for high-efficient adsorption of  
387 malachite green', *Materials Chemistry and Physics*, 240.  
388 <https://dx.doi.org/10.1016/j.matchemphys.2019.122240>.

389 Haibin, Liu, and Liu Zhenling. 2010. 'Recycling utilization patterns of coal mining waste in China', *Resources,*  
390 *Conservation and Recycling*, 54: 1331-40. <https://dx.doi.org/10.1016/j.resconrec.2010.05.005>.

391 Kong, Deshun, and Rongli Jiang. 2021. 'Preparation of NaA Zeolite from High Iron and Quartz Contents Coal  
392 Gangue by Acid Leaching—Alkali Melting Activation and Hydrothermal Synthesis', *Crystals*.  
393 <https://dx.doi.org/10.3390/cryst11101198>

394 Li, Jiayan, and Jinman Wang. 2019. 'Comprehensive utilization and environmental risks of coal gangue: A review',  
395 *Journal of Cleaner Production*. <https://dx.doi.org/10.1016/j.jclepro.2019.117946>

396 Li, Wenlei, Huixin Jin, Hongyan Xie, Duolun Wang, and Ershuai Lei. 2023. 'Utilization of electrolytic manganese  
397 residue to synthesize zeolite A and zeolite X for Mn ions adsorption', *Journal of Industrial and Engineering*  
398 *Chemistry*, 120: 147-58. <https://dx.doi.org/10.1016/j.jiec.2022.12.021>

399 Lin, Yu-Ru, Yeh-Fang Hu, Chih-Yang Huang, Huai-Ting Huang, Zhen-Hao Liao, An-Ting Lee, Yu-Sheng Wu,  
400 and Fan-Hua Nan. 2022. 'Removing Malachite Green and Leucomalachite Green From Freshwater and  
401 Seawater With Four Water Treatment Agents', *Frontiers in Environmental Science*, 10.  
402 <https://dx.doi.org/10.3389/fenvs.2022.906886>.

403 Ma, X., C. Ding, H. Yang, and X. Zhu. 2023. 'Effects of a Cellulose Aerogel Template on the Preparation and  
404 Adsorption Properties of Coal Gangue-Based Multistage Porous ZSM-5', *Materials (Basel)*, 16.  
405 <https://dx.doi.org/10.3390/ma16113896>

406 Mahreni, Mahreni, Reza Rifky Ramadhan, Muhammad Fadhil Pramadhana, Annisa Putri Permatasari, Dini  
407 Kurniawati, and Heri Septya Kusuma. 2022. 'Synthesis of Metal Organic Framework (MOF) based Ca-  
408 Alginate for adsorption of malachite green dye', *Polymer Bulletin*. <https://dx.doi.org/10.1007/s00289->  
409 [022-04086-5](https://dx.doi.org/10.1007/s00289-022-04086-5).

410 Meena, Hari Mohan, Shrikant Kukreti, and P. S. Jassal. 2024. 'Synthesis of a novel chitosan-TiO<sub>2</sub> nanocomposite  
411 as an efficient adsorbent for the removal of methylene blue cationic dye from wastewater', *Journal of*  
412 *Molecular Structure*. <https://dx.doi.org/10.1016/j.molstruc.2024.139420>

413 Rao, Zixin, Yu Chen, Kehui Qiu, Junfeng Li, Yu Jiao, Chengxiao Hu, Peicong Zhang, and Yi Huang. 2023.  
414 'Facile synthesis of NaY molecular sieve by low-temperature ultrasonic gelling method for efficien

415 t adsorption of rare-earth elements', *Materials Chemistry and Physics*, 293. <https://dx.doi.org/10.10>  
416 [16/j.matchemphys.2022.126906](https://dx.doi.org/10.1016/j.matchemphys.2022.126906)

417 Shi, Zhennan, Ling Li, Yuxiang Xiao, Yingxi Wang, Keke Sun, Hangxing Wang, and Li Liu. 2017. 'Synthesis  
418 of mixed-ligand Cu–MOFs and their adsorption of malachite green', *RSC Advances*. <https://dx.do>  
419 [i.org/10.1039/c7ra04820c](https://dx.doi.org/10.1039/c7ra04820c)

420 Uyiosa Osagie, Aigbe, Ukhurebor Kingsley Eghonghon, Onyancha Robert Birundu, Osibote Otolorin Adelaja,  
421 Darmokoesoemo Handoko, and Kusuma Heri Septya. 2021. 'Fly Ash-based Adsorbent for Adsorption of  
422 Heavy Metals and Dyes from Aqueous Solution: A Review', *Journal of Materials Research and Technology*.  
423 <https://dx.doi.org/10.1016/j.jmrt.2021.07.140>

424 Wang, Li, Junbo Wang, Aishui Yu, and Zuolong Yu. 2022. 'Removal of malachite green by electrochemical  
425 oxidation polymerization and electrochemical reduction precipitation: its kinetics and intermediates',  
426 *Journal of Solid State Electrochemistry*. <https://dx.doi.org/10.1007/s10008-022-05242-7>

427 Wu, Hao, Jingyi Yang, Lijinhong Huang, Wanfu Huang, Siyu Duan, Shangyuan Ji, Guixiang Zhang, Jun Ma, and  
428 Jiushuai Deng. 2024. 'Full-components utilization: Study on simultaneous preparation of sodalite and  
429 separation of yttrium from coal gangue by chlorination roasting process', *Separation and Purification*  
430 *Technology*, 332. <https://dx.doi.org/10.1016/j.seppur.2023.125802>.

431 Yan, Kezhou, Jiyuan Zhang, Dandan Liu, Xiang Meng, Yanxia Guo, and Fangqin Cheng. 2023. 'Feasible synthesis  
432 of magnetic zeolite from red mud and coal gangue: Preparation, transformation and application', *Powder*  
433 *Technology*. <https://dx.doi.org/10.1016/j.powtec.2023.118495>

434 Yun, Yang, Rui Gao, Huifeng Yue, Xiaofang Liu, Guangke Li, and Nan Sang. 2016. 'Polycyclic aromatic hydrocarbon  
435 (PAH)-containing soils from coal gangue stacking areas contribute to epithelial to mesenchymal transition  
436 (EMT) modulation on cancer cell metastasis', *Science of the Total Environment*.  
437 <https://dx.doi.org/10.1016/j.scitotenv.2016.12.010>

438 Zhang, Hao, Rongbo Zhao, Zhiliang Liu, Xiangchao Zhang, and Chunfang Du. 2022. 'Enhanced adsorption  
439 properties of polyoxometalates/coal gangue composite: The key role of kaolinite-rich coal gangue',  
440 *Applied Clay Science*. <https://dx.doi.org/10.1016/j.clay.2022.106730>

441 Zheng, Qinwen, Yi Zhou, Xin Liu, Meng Liu, Libing Liao, and Guocheng Lv. 2024. 'Environmental hazards and  
442 comprehensive utilization of solid waste coal gangue', *Progress in Natural Science: Materials International*.  
443 <https://dx.doi.org/10.1016/j.pnsc.2024.02.012>

444 Yuan, N., K. Tan, X. Zhang, A. Zhao & R. Guo (2022) Synthesis and adsorption performance of ultra-low silica-to-  
445 alumina ratio and hierarchical porous ZSM-5 zeolites prepared from coal gasification fine slag.  
446 *Chemosphere*, 303. <http://dx.doi.org/10.1016/j.chemosphere.2022.134839>

447 Zgureva, D., V. Stoyanova, A. Shoumkova, S. Boycheva & G. Avdeev (2020) Quasi Natural Approach for  
448 Crystallization of Zeolites from Different Fly Ashes and Their Application as Adsorbent Media for  
449 Malachite Green Removal from Polluted Waters. *Crystals*. <http://dx.doi.org/10.3390/cryst10111064>

450 Ma, X., C. Ding, H. Yang & X. Zhu (2023) Effects of a Cellulose Aerogel Template on the Preparation and  
451 Adsorption Properties of Coal Gangue-Based Multistage Porous ZSM-5. *Materials*. <http://dx.doi.org/10.3390/ma16113896>

452

453 Pereira, P., B. Ferreira, N. Oliveira, E. Nassar, K. Ciuffi, M. Vicente, R. Trujillano, V. Rives, A. Gil, S. Korili & E. de Faria  
454 (2018) Synthesis of Zeolite A from Metakaolin and Its Application in the Adsorption of Cationic Dyes.  
455 *Applied Sciences*. <http://dx.doi.org/10.3390/app8040608>

456